Dual-Reference Design for Holographic Phase Retrieval

David A. Barmherzig*, Ju Sun*, Emmanuel J. Candes*, T.J. Lane†, and Po-Nan Li*
*Stanford University
{davidbar, sunju, candes, liponan}@stanford.edu
†SLAC National Accelerator Laboratory
{tjlane}@slac.stanford.edu

***Abstract*—A new reference design is introduced for holographic coherent diffraction imaging. This consists in two references—"block" and "pinhole" shaped regions—placed adjacent to the imaging specimen. Analysis of the expected recovery error on noisy data—contaminated by Poisson shot noise—shows that this simple modification synergizes the individual references and hence leads to uniformly superior performance over single-reference schemes. Numerical experiments on simulated data confirm the theoretical prediction, and the proposed dual-reference scheme achieves a smaller recovery error than leading single-reference schemes. A full version of this paper is available at https://arxiv.org/abs/1902.02492.**

I. Introduction

A. Holographic CDI and Holographic Phase Retrieval

Coherent Diffraction Imaging, or CDI, is a scientific imaging technique used for resolving nanoscale scientific specimens, such as macroviruses, proteins, and crystals [1]. In CDI, a coherent radiation source (often an X-ray beam) is diffracted after being incident upon a specimen. The resulting photon flux is then measured at a far-field detector, and the measured data are approximately proportional to the squared magnitudes of the Fourier transform of the electric field within the diffraction area. One can then determine the specimen's electron density by solving the *phase retrieval* problem, the mathematical inverse problem of recovering a signal from its squared Fourier magnitudes.

In a variant of CDI known as Holographic CDI, a "reference" portion of the diffraction area is a priori known from experimental design (e.g. see Fig. 1). Typically, the reference portion is simply a geometric shape cut out from the apparatus surrounding the specimen. The resulting inverse problem, in which a portion of the signal to be recovered is already known, is the *holographic phase retrieval* problem.

For any reference choice satisfying mild assumptions, solving the holographic phase retrieval problem amounts to solving a structured linear system [3]. However, different reference choices will lead to different noise stability performances. Particularly, our previous work [3] revealed, both theoretically and empirically, the relative merits of two popular references: given the squared Fourier magnitudes, the block reference R_B (see Fig. 2b) performs favorably on low-frequency dominant spectrum, whereas the pinhole reference (see Fig. 2c) has an edge for flat spectra. It is a natural question if the merits can be combined, and how.

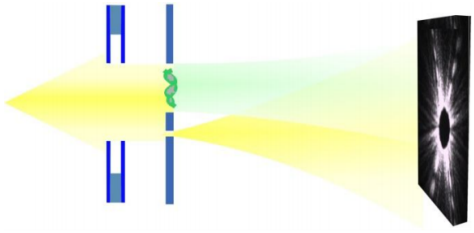

Fig. 1: Holographic CDI schematic. The upper portion of the diffraction area contains the imaging specimen of interest, and the lower portion consists of a known "reference" shape. Image courtesy of [2].

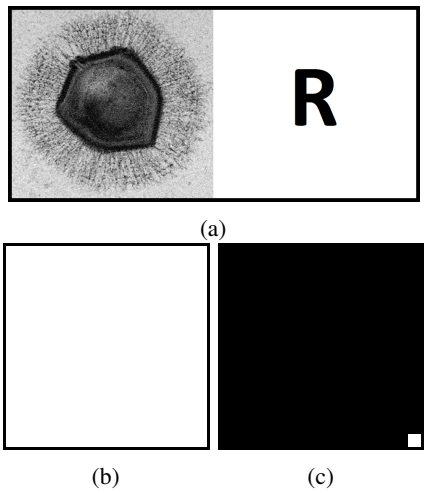

Fig. 2: Schematic of the diffraction area in Holographic CDI containing a specimen and a known (single) reference. Two popular choices for the reference R are the block reference (Fig. 2b) and the pinhole reference (Fig. 2c). The specimen shown is the Mimivirus, courtesy of [4].

B. Our Contributions

In this paper, we answer the question in the affirmative and show that a simple augmentation of the block and pinhole references actually works as desired. From hindsight, this is still a bit surprising, as the recovery error depends on the reference choice in a complicated manner; see Eq. (IV.2). Both theoretical (Section III) and empirical (Section V) results confirm the

effectiveness of the proposed augmentation scheme.

II. Dual-Reference Design

Definition II.1. *The block reference $R_B \in \mathbb{R}^{n\times n}$ and the pinhole reference $R_P \in \mathbb{R}^{n\times n}$ are defined respectively by*

$$R_B(t_1,t_2) = 1, \quad t_1,t_2 \in \{0,\dots,n-1\}, \tag{II.1}$$

and

$$R_P(t_1,t_2) = \begin{cases} 1, & t_1 = t_2 = n-1 \\ 0, & \text{otherwise.} \end{cases} \tag{II.2}$$

They are shown in Fig. 2b and Fig. 2c, respectively. Suppose that $X \in \mathbb{C}^{n\times n}$ is an "unknown" specimen. Consider $\mathcal{X} \in \mathbb{C}^{(2n)\times(2n)}$ given by:

$$\mathcal{X} = \begin{bmatrix} X & R_B \\ R_P & \mathbf{0}_{n\times n} \end{bmatrix}, \tag{II.3}$$

where $\mathbf{0}_{n\times n}$ is the $n \times n$ matrix of zeros. [1] We shall assume that the magnitudes of the entries of X are within the interval $[0,1]$. By this convention, 0 values represent areas where the incoming beam is entirely blocked, and 1 values represent areas where the incoming beam passes through unimpeded—which would be "empty space".

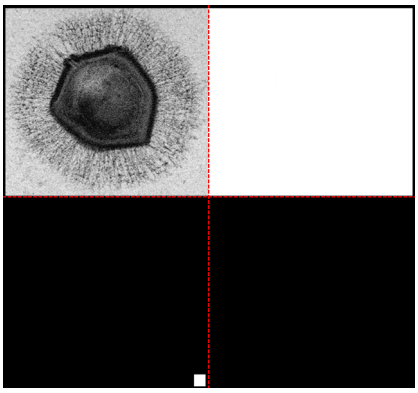

Fig. 3: Dual-Reference Scheme. The red dotted line (added for illustration purposes) separates the four quadrants of the setup, as described by Eq. (II.3). The specimen shown is the Mimivirus, courtesy of [4].

III. Recovery Algorithm

Suppose that $m \geq 4n-1$ and that $Y = |\widehat{\mathcal{X}}|^2 \in \mathbb{C}^{m\times m}$ are the $m \times m$ oversampled Fourier transform magnitudes[2] of $\mathcal{X}$. We seek to recover X from $\widetilde{Y}$, which is a possibly noise-corrupted version of Y. We outline the following recovery algorithm, which is the referenced deconvolution algorithm of [3] adapted to our current dual-reference scheme.

1) Given $\widetilde{Y}$, apply an inverse Fourier transform ($\mathbb{C}^{m\times m} \mapsto \mathbb{C}^{(4n-1)\times(4n-1)}$) to obtain $\widetilde{A}_{\mathcal{X}}$, the noisy autocorrelation of $\mathcal{X}$.[3] This can be expressed as $\widetilde{A}_{\mathcal{X}} = \frac{1}{m^2} F^* \widetilde{Y} (F^*)^T$, where $F \in \mathbb{C}^{m\times(4n-1)}$ is given by $F(k,t) = e^{-2\pi i k t/m} \;\; \forall \;\; (k,t) \in \{0,\dots,m-1\} \times \{-(2n-1),\dots,2n-1\}$.
2) Let $\mathcal{P}_1 = [\mathbf{0}_{n\times n}, I_n, \mathbf{0}_{n\times(2n-1)}]$ and $\mathcal{P}_2 = [I_n, \mathbf{0}_{n\times(3n-1)}]$. It follows that $\mathcal{P}_1 \widetilde{A}_{\mathcal{X}} \mathcal{P}_2^\top \in \mathbb{R}^{n\times n}$ (resp., $\mathcal{P}_2 \widetilde{A}_{\mathcal{X}} \mathcal{P}_1^\top \in \mathbb{R}^{n\times n}$) is (without noise) equal to the top-left quadrant of the cross-correlation of X and R_B (resp., X and R_P). We thus denote this as $\widetilde{C}^{\diamond}_{[X,R_B]}$ (resp., $\widetilde{C}^{\diamond}_{[X,R_P]}$).
3) Let M_{R_B} (resp., M_{R_P}) $\in \mathbb{R}^{n^2\times n^2}$ be the matrix satisfying $M_{R_B} \operatorname{vec}(X) = \operatorname{vec}(C^{\diamond}_{[X,R_B]})$ (resp., $M_{R_P} \operatorname{vec}(X) = \operatorname{vec}(C^{\diamond}_{[X,R_P]})$).[4] It follows that $M_{R_B} = \mathbf{1}_L \otimes \mathbf{1}_L$, where $\mathbf{1}_L \in \mathbb{R}^{n\times n}$ is the lower-triangular matrix consisting of all ones on and below the main diagonal, and that $M_{R_P} = I_{n^2}$. Let $M = [M_{R_B}; M_{R_P}]$ and $b = [\operatorname{vec}(\widetilde{C}^{\diamond}_{[X,R_B]}); \operatorname{vec}(\widetilde{C}^{\diamond}_{[X,R_P]})]$. The signal X is estimated as the solution to the least-squares problem

$$X^* = \underset{X\in\mathbb{C}^{n\times n}}{\arg\min} \; \|M \operatorname{vec}(X) - b\|^2 .$$

Analytically, this is given by

$$\operatorname{vec}(X^*) = M^\dagger b = (M^T M)^{-1} M^T b.$$

Combining these steps and the well-known matrix Kronecker product identity that $A = BCD \iff \operatorname{vec}(A) = (D^T \otimes B)\operatorname{vec}(C)$, it then follows that

$$\operatorname{vec}(X^*) = T_{R_{B,P}} \operatorname{vec}(Y^*), \tag{III.1}$$

where

$$T_{R_{B,P}} = \frac{1}{m^2} M^\dagger \begin{bmatrix} \mathcal{P}_2 F^* \otimes \mathcal{P}_1 F^* \\ \mathcal{P}_1 F^* \otimes \mathcal{P}_2 F^* \end{bmatrix}. \tag{III.2}$$

Note that this algorithm gives a linear relationship between $\widetilde{X}$ and $\widetilde{Y}$. In the noiseless setting, it exactly recovers the signal X.

IV. Error Analysis

For any data $\widetilde{Y}$ following a known probability distribution, it follows from Eq. (III.1) that

$$\mathbb{E}\|\widetilde{X} - X\|_F^2 = \left\langle T_R^* T_R, \mathbb{E}\left[\operatorname{vec}\left(\widetilde{Y}\right) - \operatorname{vec}(Y)\right]\left[\operatorname{vec}\left(\widetilde{Y}\right) - \operatorname{vec}(Y)\right]^*\right\rangle,$$

where $\|\cdot\|_F^2$ denotes the Frobenius norm, and $\langle\cdot,\cdot\rangle$ denotes the Frobenius inner product.

In CDI, detector measurements of photon flux are subject to quantum shot noise. This is due to intrinsic quantum fluctuations which cannot be removed by any measurement

[1] In (holographic) phase retrieval, the specimen X and the measurements $|\mathcal{F}(X)|^2$ are often also formulated as continuous functions to better model the physical nature of the problem. Thanks to the close connections of various components of discrete and continuous Fourier analysis, the discrete formulation can be thought of as approximation to the uniform sampling of the continuous version. See full version of the paper for detailed justification.

[2] Here, the absolute value notation is understood in the pointwise sense.

[3] It is well-known that the inverse Fourier transform of the squared Fourier magnitudes (with sufficient oversampling) of a signal is equal to the signal's autocorrelation [5].

[4] The cross-correlations are linear in X, and hence such M_{R_B} and M_{R_P} exist for the noiseless cross-correlations $C^{\diamond}_{[X,R_B]}$ and $C^{\diamond}_{[X,R_P]}$.

system. The resulting photon flux measurements follow the Poisson shot noise distribution given by

$$\widetilde{Y} \sim_{\text{ind}} \frac{\|Y\|_1}{N_p}\text{Pois}\Big(\frac{N_p}{\|Y\|_1}Y\Big), \tag{IV.1}$$

where N_p is the expected (or nominal) number of photons reaching the detector, and $\|Y\|_1$ is understood as the ℓ_1 norm of a vectorized version of Y [6]. In view of Sec. 3 of [3] and Eq. (III.1), we have

$$\mathbb{E}\|\widetilde{X} - X\|_F^2 = \frac{\|Y\|_1}{N_p}\left\langle S_{R_{B,P}}, Y\right\rangle, \tag{IV.2}$$

where

$$S_{R_{B,P}} = \text{reshape}\big(\,\text{diag}(T_R^* T_R), m, m\big), \tag{IV.3}$$

and $\text{reshape}(\cdot, m, m)$ is the columnwise vector-to-matrix reshaping operator.

An analytical expression for $S_{R_{B,P}}$ can be derived, which follows from the singular value of decomposition of $\mathbf{1}_L$ together with elementary properties of the Kronecker product.

Lemma IV.1 (Chapter 1 of [7])**.** *The singular value decomposition $\mathbf{1}_L = U\Sigma V^T$ is such that for $t, s \in \{0, \ldots, n-1\}$, U and V have columns given by*

$$u_s(t) = \frac{1}{\sqrt{\frac{n}{2}+\frac{1}{4}}}\sin\left\{\frac{(s+\frac{1}{2})(t+\frac{1}{2})}{n+\frac{1}{2}}\pi\right\},$$

$$v_s(t) = \frac{1}{\sqrt{\frac{n}{2}+\frac{1}{4}}}\cos\left\{\frac{(s+\frac{1}{2})(t+\frac{1}{2})}{n+\frac{1}{2}}\pi\right\},$$

respectively, and

$$\Sigma(s,s) = \left[2 - 2\cos\left(\frac{s+\frac{1}{2}}{n+\frac{1}{2}}\pi\right)\right]^{-1/2}.$$

Proposition IV.2. *For any $k_1, k_2 \in \{0, \ldots, m-1\}$, $S_{R_{B,P}}(k_1, k_2)$ is equal to*

$$\frac{1}{m^4}\sum_{r,s=0}^{n-1}\Big|\frac{\sigma_r\sigma_s}{\sigma_r^2\sigma_s^2+1}u_r^\top\left(\mathcal{P}_2F^*\right)_{k_1}u_s^\top\left(\mathcal{P}_1F^*\right)_{k_2}$$
$$+\frac{1}{\sigma_r^2\sigma_s^2+1}v_r^\top\left(\mathcal{P}_1F^*\right)_{k_1}v_s^\top\left(\mathcal{P}_2F^*\right)_{k_2}\Big|^2, \tag{IV.4}$$

where the notation $(\cdot)_k$ above is used to denote the k^{th} column of a matrix.

In the expected squared recovery error Eq. (IV.2), both Y and S_R depend on the reference scheme in use. Empirically, for low-frequency dominant X with typical $[0,1]$ values (e.g., images shown in Fig. 2 and Fig. 6, typical CDI specimens), Y will have a similar spectrum to X (up to small variation in the order of magnitude) for the various reference schemes of interest; see Fig. 4. This stability property of spectrum can be formally established for the single-reference setup $[X, R]$ by expanding $|\widehat{[X,R]}|^2$ [3], and likewise for our dual-reference setup $\mathcal{X}$. In contrast, the weighting factors in S_R can vary by several orders of magnitudes for different reference schemes, as shown in Fig. 5. Hence, the influence of the reference scheme on the expected squared error is largely determined by S_R.

In Fig. 5, we compare the S_R's for the single-reference setup (either the pinhole or the block reference) with that of our dual-reference setup. For the single-reference setup $[X, R]$, [3] showed that among three popular reference choices, the block and pinhole references perform best for low-frequency dominant Y and flat-spectrum Y, respectively. The elegant idea of including the two references simultaneously and solving the resulting stacked linear system helps combine the benefits. Indeed, as can be seen from Fig. 5, $S_{R_{B,P}}$ approximates the minimum of S_{R_B} and S_{R_P} uniformly over the entire frequency spectrum.

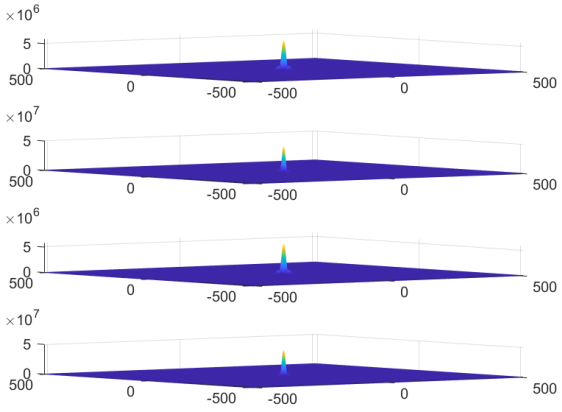

Fig. 4: Top to bottom: squared magnitudes of the Fourier transform of the mimivirus [4] itself, and that of combined with the block, pinhole, and dual-references, respectively (with $n = 64$, and $m = 1024$). These four spectra exhibit similar low-frequency dominance, and have entries of similar orders of magnitude.

V. Numerical Simulations

We observe in numerical simulation of CDI experiments that the dual-reference provides smaller recovery error than does the leading single-reference schemes with the block or pinhole reference. A comparison of the recovery error is provided in Table I for the Mimivirus image [4] (Fig. 2), the influenza virus and stroma cell tubules images (shown in Fig. 6).

VI. Conclusion

We have proposed a novel dual-reference scheme for Holographic CDI, together with a recovery algorithm which provides exact recovery in the noiseless setting. For data corrupted by Poisson shot noise, the dual-reference combines the best features of the block and pinhole references. Numerical experiments on simulated CDI data show the dual-reference scheme provides a smaller recovery error than the leading (single) reference schemes.

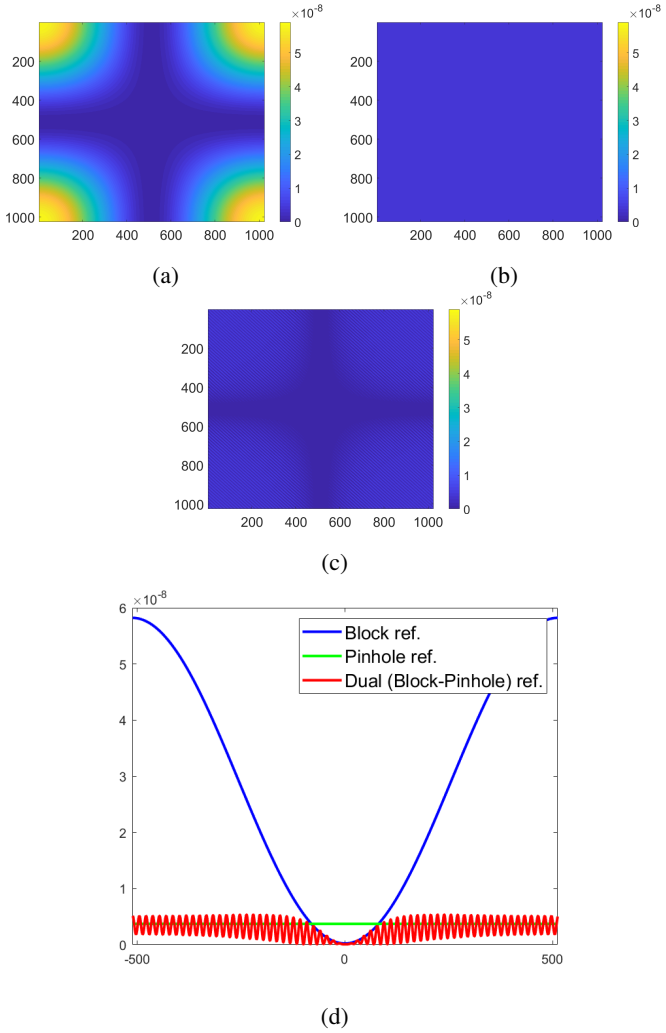

Fig. 5: The top row shows colormap plots of the weighting factors S_R for the block, pinhole, and dual references, respectively, when $n = 64$ and $m = 1024$. The bottom plot shows the three weighting factors along the (four identical) bordering cross-sections of the colormap plots.

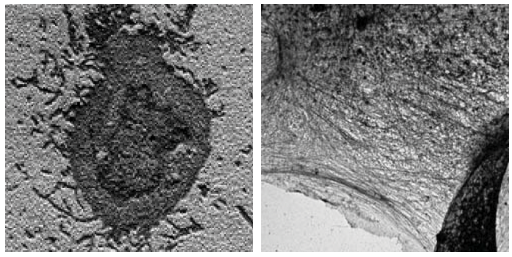

Fig. 6: Influenza and stroma cell tubules images used for numerical simulations in Table I, courtesy of [8].

TABLE I: Empirical and expected values for the relative squared errors $\|X^\star - X\|_F^2 / \|X\|_F^2$. Recorded error values are scaled by 10^{-4}. Test images X of size 64×64 pixels are the Mimivirus (Fig. 2), Influenza, and Tubules images (Fig. 6). Simulated photon flux data is of size 1024×1024, with $N_p = 1000(1024^2)$ (i.e. 1000 photons per pixel).

	Empirical Err.	**Expected Err.**
Mimivirus		
Block Ref.	3.70	3.79
Pinhole Ref.	46.9	63.8
Dual Ref. (Block-Pinhole)	1.51	1.45
HIO (no ref.)	93.7	N/A
HIO (with block ref.)	42.8	N/A
HIO (with pinhole ref.)	168.1	N/A
Influenza		
Block Ref.	18.7	18.5
Pinhole Ref.	50.7	31.4
Dual Ref. (Block-Pinhole)	4.64	4.70
HIO (no ref.)	695.7	N/A
HIO (with block ref.)	219.6	N/A
HIO (with pinhole ref.)	401.1	N/A
Tubules		
Block Ref.	9.19	8.91
Pinhole Ref.	23.1	44.1
Dual Ref. (Block-Pinhole)	2.78	2.63
HIO (no ref.)	1607.0	N/A
HIO (with block ref.)	110.8	N/A
HIO (with pinhole ref.)	2204.8	N/A

ACKNOWLEDGMENTS

The authors are grateful to Walter Murray and Gordon Wetzstein for many guiding discussions throughout this research. We thank the anonymous reviewers for their insightful feedback.

REFERENCES

[1] J. Miao, P. Charalambous, J. Kirz, and D. Sayre, "Extending the methodology of X-ray crystallography to allow imaging of micrometre-sized non-crystalline specimens," *Nature*, vol. 400, pp. 342–344, jul 1999.

[2] M. Saliba, T. Latychevskaia, J. Longchamp, and H. Fink, "Fourier Transform Holography: A Lensless Non-Destructive Imaging Technique," *Microscopy and Microanalysis*, vol. 18, no. S2, pp. 564–565, 2012.

[3] D. A. Barmherzig, J. Sun, E. J. Candes, T. J. Lane, and P.-N. Li, "Holographic Phase Retrieval and Optimal Reference Design," *arXiv e-prints 1901.06453*, Jan. 2019.

[4] E. Ghigo, J. Kartenbeck, P. Lien, L. Pelkmans, C. Capo, J.-L. Mege, and D. Raoult, "Ameobal Pathogen Mimivirus Infects Macrophages through Phagocytosis," *PLOS Pathogens*, vol. 4, no. 6, pp. 1–17, 2008. [Online]. Available: https://doi.org/10.1371/journal.ppat.1000087

[5] A. V. Oppenheim and R. W. Schafer, *Discrete-Time Signal Processing*, 3rd ed. Upper Saddle River, NJ, USA: Prentice Hall Press, 2009.

[6] I. S. Wahyutama, G. K. Tadesse, A. Tünnermann, J. Limpert, and J. Rothhardt, "Influence of detector noise in holographic imaging with limited photon flux," *Opt. Express*, vol. 24, no. 19, pp. 22 013–22 027, sep 2016. [Online]. Available: http://www.opticsexpress.org/abstract.cfm?URI=oe-24-19-22013

[7] G. Strang, *Computational Science and Engineering*. Wellesley, MA, USA: PWellesley-Cambridge Press, 2012.

[8] D. Kim, T. J. Deerinck, Y. M. Sigal, H. P. Babcock, M. H. Ellisman, and X. Zhuang, "Correlative stochastic optical reconstruction microscopy and electron microscopy," *PLOS ONE*, vol. 10, no. 4, pp. 1–20, 04 2015. [Online]. Available: https://doi.org/10.1371/journal.pone.0124581